Supporting Information

Optimizing the morphology of all-polymer solar cells for enhanced photovoltaic performance and thermal stability

Kang An[1,#], Wenkai Zhong[2,#], Chunguang Zhu[1,#], Feng Peng[3], Lei Xu[1], Zhiwei Lin[4], Lei Wang[5], Cheng Zhou[1], Lei Ying[1,*], Ning Li[1,*] and Fei Huang[1]

[1]Institute of Polymer Optoelectronic Materials and Devices, State Key Laboratory of Luminescent Materials and Devices, South China University of Technology, Guangzhou 510640, China

[2]Frontiers Science Center for Transformative Molecules, Center of Hydrogen Science, and School of Chemistry and Chemical Engineering, Shanghai Jiao Tong University, Shanghai 200240, China

[3]South China Institute of Collaborative Innovation, Dongguan 523808, China

[4]South China Advanced Institute for Soft Matter Science and Technology, School of Emergent Soft Matter, South China University of Technology, Guangzhou 510640, China

[5]School of Light Industry and Engineering &State Key Laboratory of Pulp & Paper Engineering, South China University of Technology, Guangzhou 510640, China

[#] Kang An, Wenkai Zhong, and Chunguang Zhu contributed equally to this work.

[*]E-mail: msleiying@scut.edu.cn; ningli2022@scut.edu.cn

Experimental section

Materials

PTzBI-oF (Mn = 35.39 kDa, 2.36) and PS1 (Mn = 12.65 kDa, 2.16) were synthesized according to our previously reports[1,2]. PNDIT-F3N-Br was purchased from VOLT-AMP OPTOELECTRONICS TECH. CO., LTD. The aqueous dispersion of PEDOT:PSS (4083) buffer layer (batch: 9006378404) was purchased from Heraeus, Germany. All solvents and chemicals were ordered from Sigma-Aldrich and used without further purification.

All-PSCs fabrication

All-polymer solar cells (all-PSCs) were manufactured with the conventional structure of ITO/PEDOT:PSS/Active layer/PNDIT-F3N-Br/Ag. Patterned ITO substrates were ultrasonically cleaned with detergent, deionized water, and isopropanol for 30 minutes respectively and dried in an oven of 65 ℃ overnight. Subsequently, the ITO substrates were treated with vacuum plasma cleaning for 2 min. Then, the PEDOT:PSS buffer layer, filtered with 13 mm/0.22 μm aqueous polyethersulfone membrane syringe filters, was spin-coated on ITO substrate with 3000 r/min for 30 s, and baked at 150 °C for 15 min in air. For the SD device, the polymer donor PTzBI-oF dissolved in chloroform (CF) at a concentration of 8.5 mg/mL was spin-coated onto the PEDOT:PSS buffer layer with the rotate speed varied from 1200 to 2300 r/min to give the thickness ranging from 40 to 60 nm. Then, the PS1 in CF solution (8.5 and 9.5 mg/mL), with the volume ratio of dibenzyl ether (DBE) from 0 to 2%, was subsequently spin-coated on the top of PTzBI-oF layer at from 1500 to 3000 r/min. Thermal annealing treatment was performed at 100 °C for 10 minutes after finished above two layers. The thicknesses of active layers ranged from 90 to 130 nm was determined by a Bruker Dektak XT profilometer. The blend-casting all-PSCs was constructed consistent with our previous reported procedures[2]. A methanol solution of PNDIT-F3N-Br at a concentration of 0.5 mg mL^{-1} was spin-coated onto the photoactive layer at 2000 r/min for 25 s. Finally, silver electrodes of 100 nm were deposited on top of the PNDIT-F3N-Br buffer layer through a shadow mask under a vacuum about 1×10^{-7} mbar. The effective area was 0.0516 cm^2, further defined as 0.04 with a non-refractive mask.

Charge-only devices fabrication

The structure for hole-only and electron-only devices was ITO/PEDOT:PSS/Active layer/MoO_x/Ag and ITO/ZnO/Active layer/PNDIT-F3N-Br/Ag, respectively. The fabricating process of active layers was consistent those corresponding all-PSCs. Mobilities are illustrated with the Mott-Gurney equation:

$$J = 9\varepsilon_0\varepsilon_r\mu V^2/8d^3$$

where J is the space charge limited current, ε_0 is the vacuum permittivity (8.85×10^{-12} F/m), ε_r is the permittivity for active layers, μ is the charge mobility, and d is the

thickness of active layers. The effective voltage (V) was obtained by the equation: $V = V_{appl} - V_{bi} - V_s$, where the built-in voltage (V_{bi}) and the voltage drop (V_s) were deducted from the applied voltage (V_{appl}) of devices. Hole and electron mobilities were integrated from the slope of the $J^{1/2}$–V curves.

Instruments and characterizations

Ultraviolet–visible (UV–vis) absorption was measured with a SHIMADZU UV-3600 spectrophotometer. Photoluminescence (PL) was acquired with a FLS920 spectrofluorimeter (Edinburgh Instruments) by a xenon arc lamp (150 W). The $J - V$ curves were measured under a computer controlled Keithley 2400 sourcemeter under 100 mW/cm^2, AM 1.5G solar simulator (Enlitech SS-F5). The light intensity was calibrated by a standard silicon solar cell (certified by NREL) to give a range from 0.99 to 1.01 sun. The EQE spectra were received from a commercial QE measurement system (Taiwan, Enlitech, QE-R3011). Hole and electron-only devices were recorded with a Keithley 236 sourcemeter under a dark chamber. Impedance spectra was obtained by KEYSIGHT impedance analyzer E4990A (20 Hz-10 MHz). For the transient photocurrent (TPC) and the transient photovoltage (TPV) measurements, photogenerated charge carriers were excited at 580 nm by a mode-locked Ti:sapphire oscillator (SpectraPhysics Spitfire Ace) with a pulse width of 120 fs and the repetition rate of 1 kHz. TPC signal was recorded with an oscilloscope (Tektronix TDS 3052C) with a 50 Ω resistor. TPV signal was recorded on a 1 MΩ resistor, under an LED light. Tapping-mode AFM images were obtained by a Bruker Multimode 8 Microscope. TEM images were received from the JEM 2100F Microscope. GIWAXS characterization was performed on MetalJet-D2 X-ray Source (Excillum). The scattering signal of was received from a Pilatus 3R 1M detector (Dectris) with a pixel size of 0.172 × 0.172 mm^2. The incidence angle was 0.2°, exhibiting the optimized signal-to-background ratio. Diffraction signals were collected with 1800 s exposure time and the acquired two images were merged together. The measured samples were spin-coated on silicon wafer

substrates coated with PEDOT:PSS layer, and the fabricated process were identical to corresponding all-PSCs.

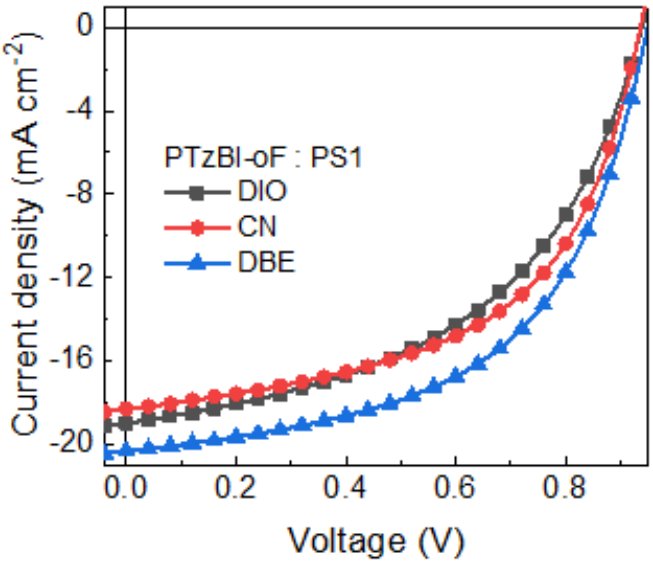

Figs. 1. Summary of SD all-PSCs based on PTzBI-oF and PS1 with different additives.

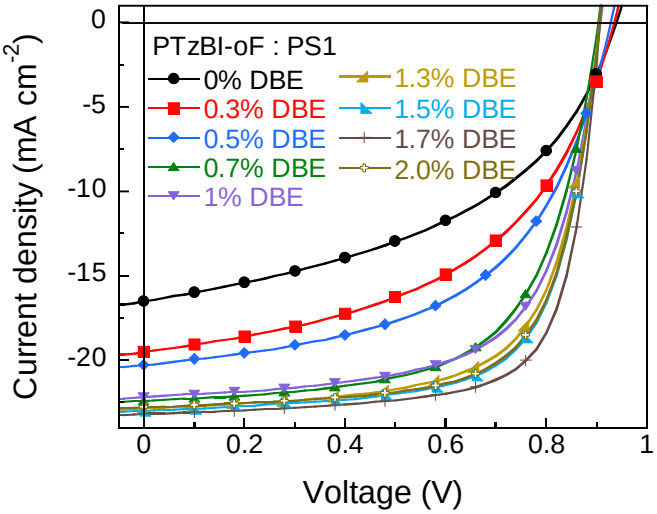

Figs. 2. Summary of SD all-PSCs based on PTzBI-oF and PS1 with different DBE contents.

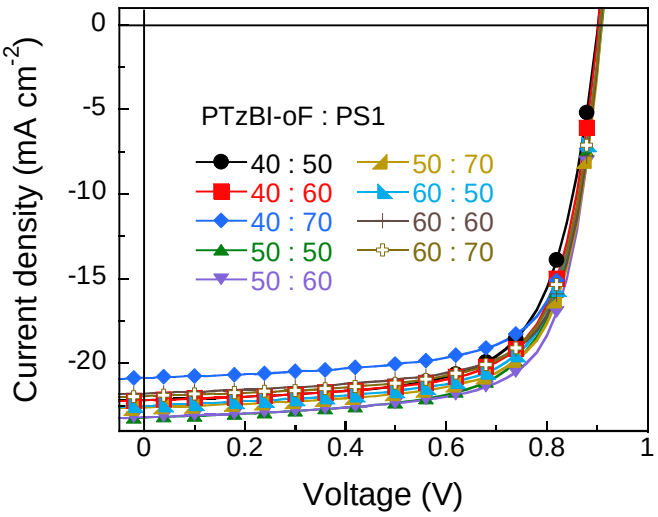

Figs. 3. Summary of SD all-PSCs based on PTzBI-oF and PS1 at optimized DBE contents with different thickness.

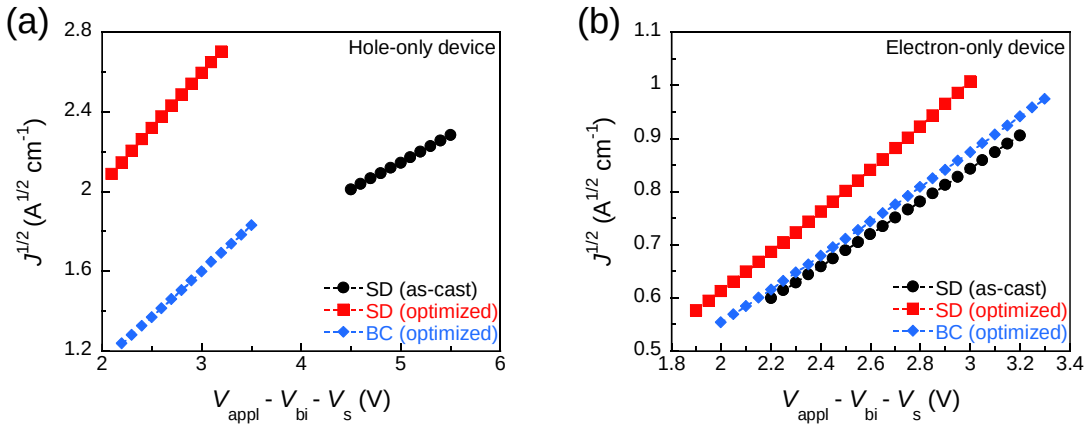

Figs. 4. The current density versus applied voltage characteristics for (a) hole-only and (b) electron-only devices.

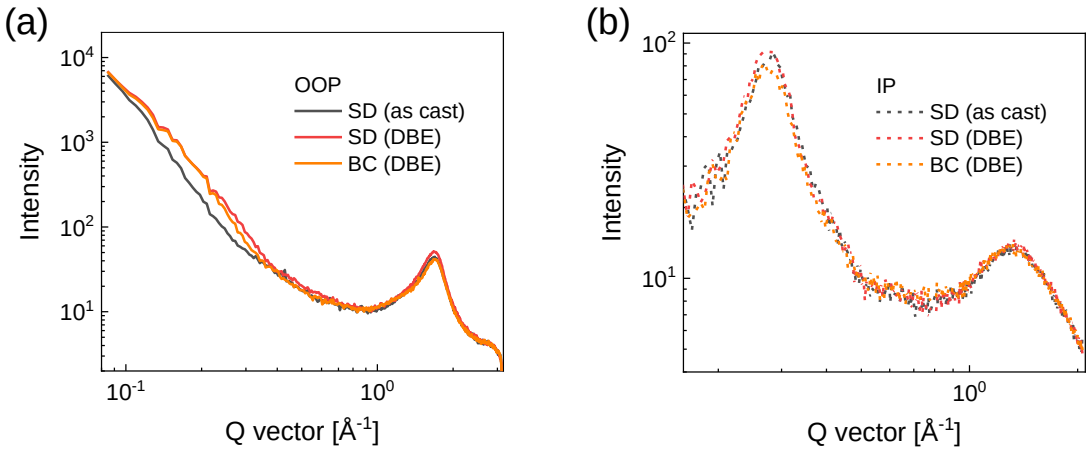

Figs. 5. Sector averaged curves in the OOP (solid lines) and IP (dotted lines) directions.

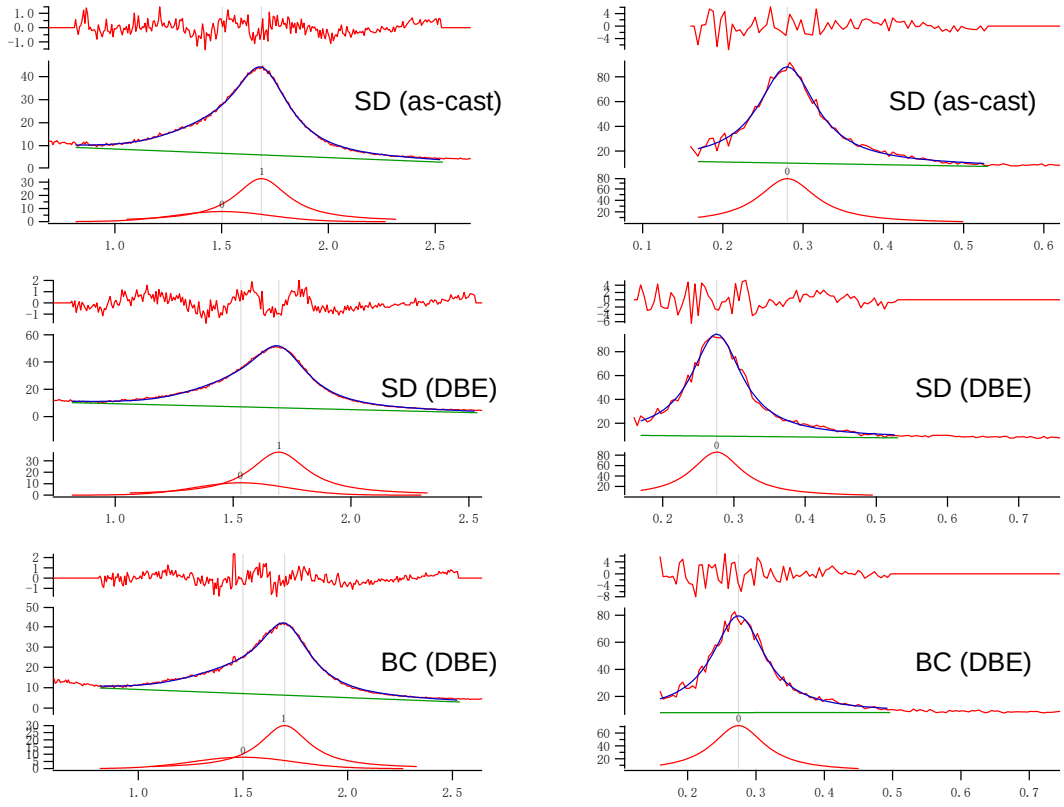

Figs. 6. Curves fitting results of lamellar stacking and π-π stacking reflections.

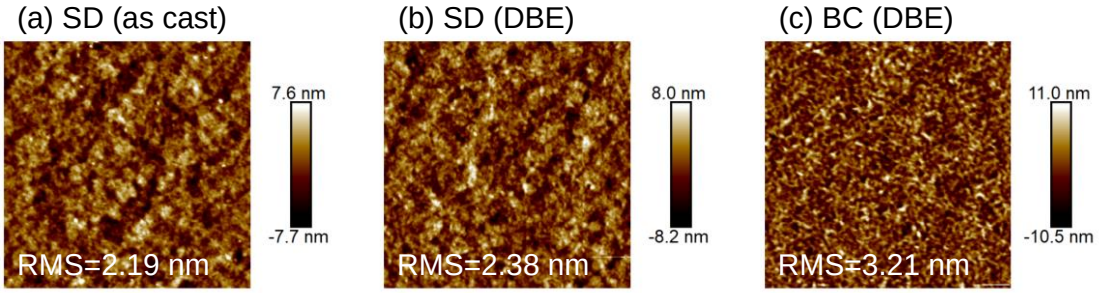

Figs. 7. Tapping-mode AFM height images (5 × 5 μm^2) for SD_as cast (a), SD_DBE (b) and BC_DBE (c) blends.

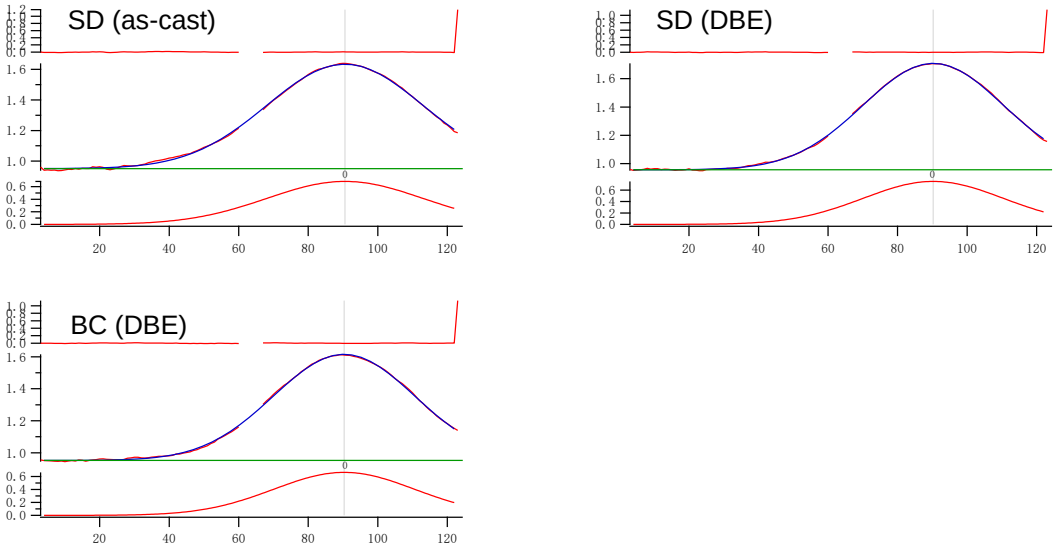

Figs. 8. Curves fitting results pole figures for the π-π stacking reflections.

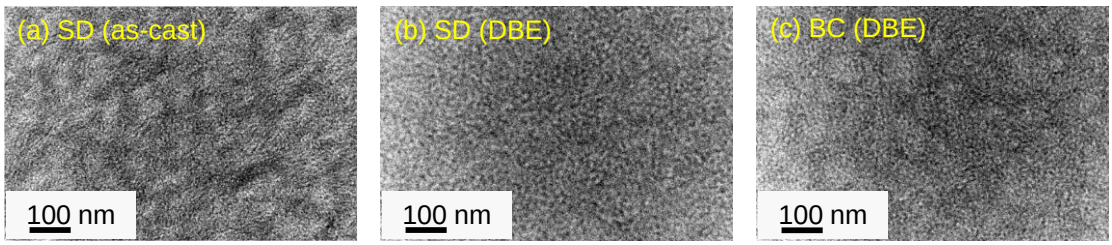

Figs. 9. Transmission electron microscopy (TEM) images for (a) SD (as cast), (b) SD (DBE) and (c) BC (DBE) blends.

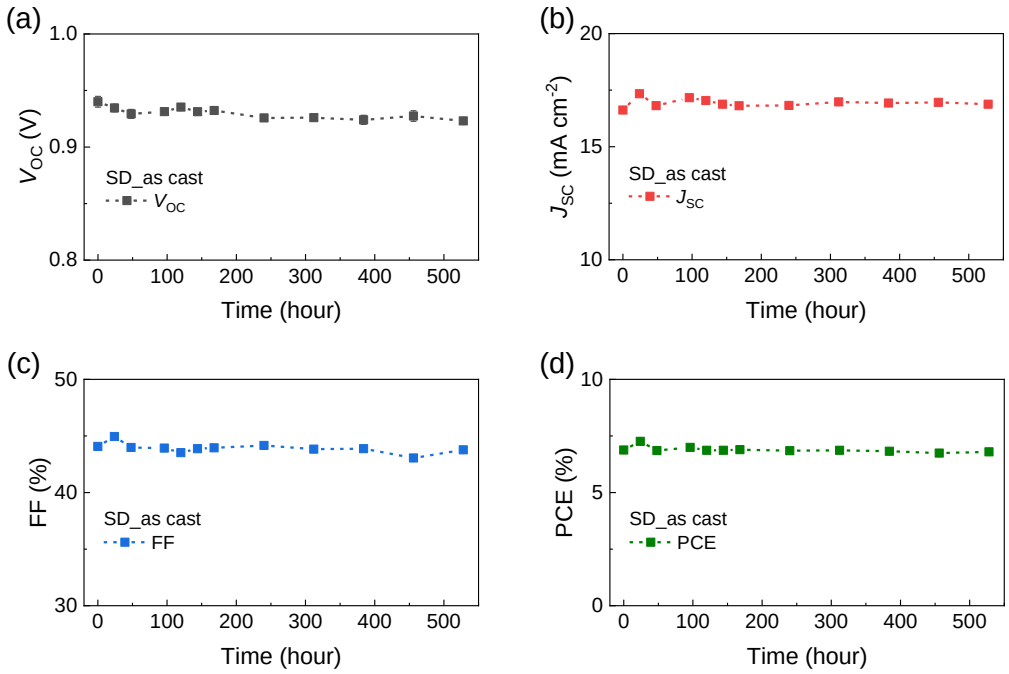

Figs. 10. Degradation parameters for as cast PTzBI-oF:PS1 based all-PSCs constructed with sequential deposition methods continuously thermal aging at 65 °C.

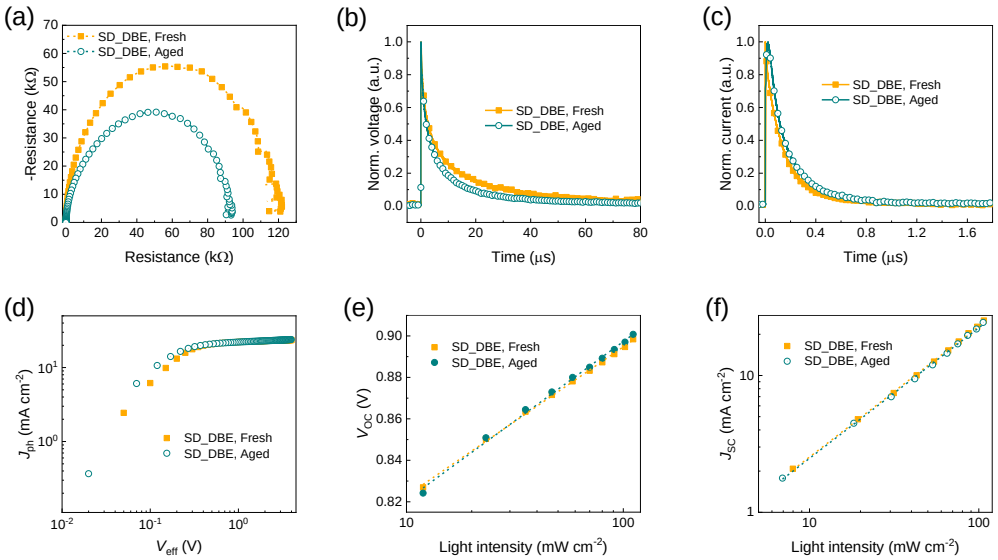

Figs. 11. Impedance spectra (a), normalized transient photovoltage (b) and transient photocurrent curves (c), J_{ph}–V_{eff} characteristics (d), dependence of V_{OC} (e) and J_{SC} (f) on light intensity (P_{light}) measurements for fresh and aged PTzBI-oF:PS1 all-PSCs fabricated by the sequential deposition method.

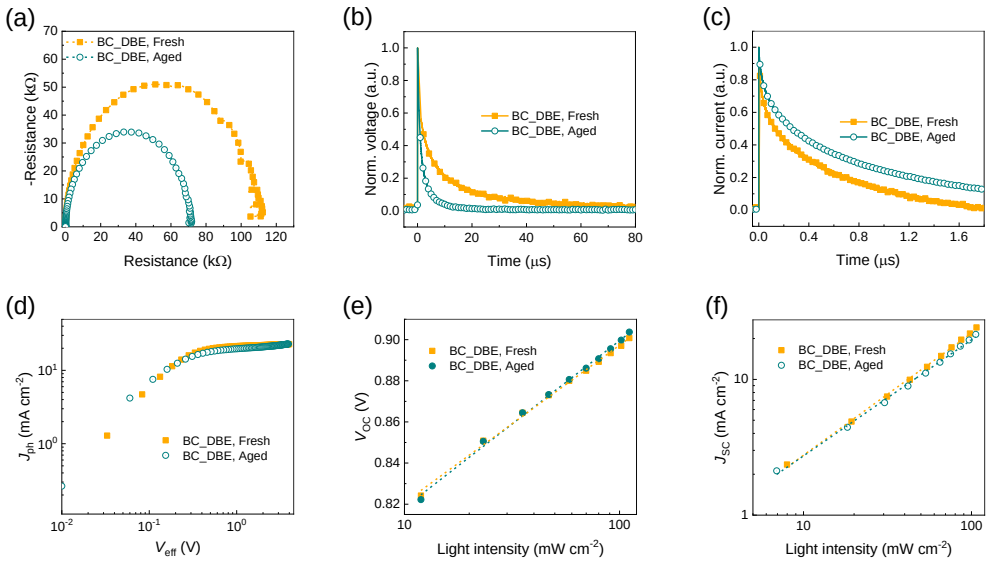

Figs. 12. Impedance spectra (a), normalized transient photovoltage (b) and transient photocurrent curves (c), J_{ph}–V_{eff} characteristics (d), dependence of V_{OC} (e) and J_{SC} (f) on light intensity (P_{light}) measurements for fresh and aged PTzBI-oF:PS1 all-PSCs fabricated by the blend casting method.

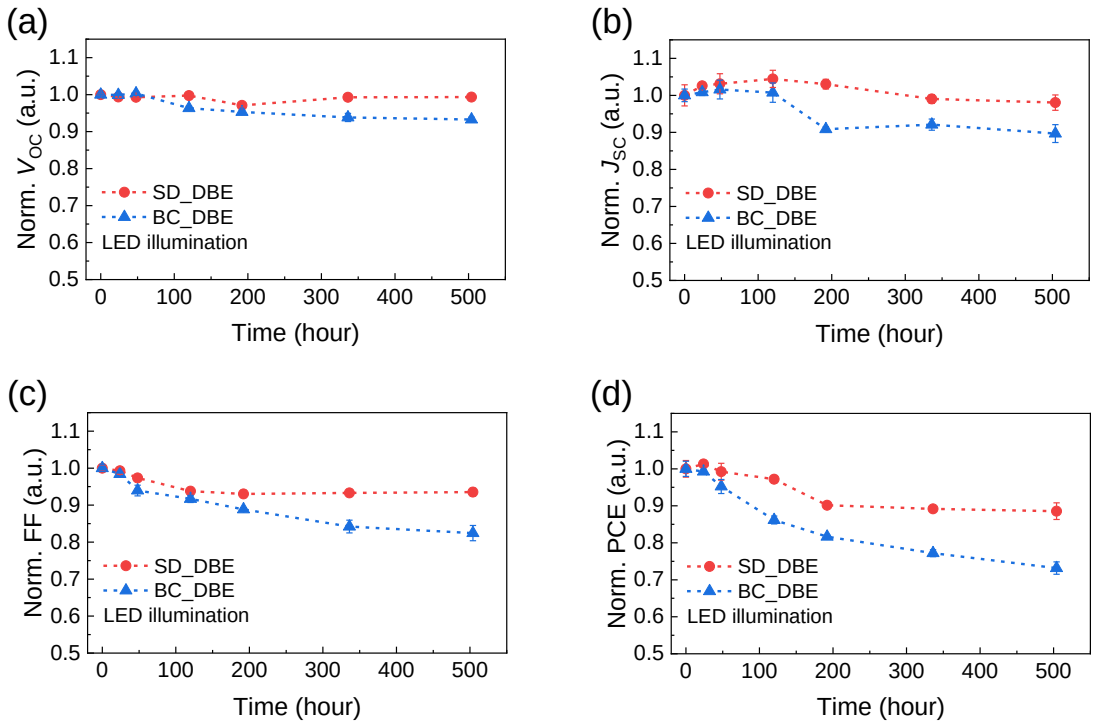

Figs. 13. Stability performances of SD_DBE and BC_DBE devices under continuous light aging (LED light source, 6500 K, 0.7 sun calibrated by Si detector, 45 ℃ at device surface).

Table S1. Photoluminescence (PL) quenching efficiency and lifetime of corresponding films.

Active layer	PL quenching efficiency (%)
PTzBI-oF	100
BC (PTzBI-oF:PS1)	91.47
SD (PTzBI-oF/PS1)	87.41
PS1	100
BC (PTzBI-oF:PS1)	93.14
SD (PTzBI-oF/PS1)	90.05

Table S2. Device parameters of SD all-PSCs based on PTzBI-oF and PS1 with different additives.

Additive	V_{OC} (V)	J_{SC} (mA/cm^2)	FF (%)	PCE (%)
DIO	0.938	19.00	48.64	8.68
CN	0.936	18.32	54.08	9.27
DBE	0.928	20.30	54.01	10.18

Table S3. Device parameters of SD all-PSCs based on PTzBI-oF and PS1 with different DBE contents.

DBE (%)	V_{OC} (V)	J_{SC} (mA/cm^2)	FF (%)	PCE (%)
0	0.940	16.51	45.94	7.13
0.3	0.935	19.51	49.98	9.12
0.5	0.928	20.30	54.01	10.18
0.7	0.904	22.40	63.24	12.81
1.0	0.908	22.17	64.94	13.07
1.3	0.906	22.87	67.03	13.89
1.5	0.906	22.99	68.75	14.33
1.7	0.906	23.18	72.35	15.21
2.0	0.906	22.77	68.90	14.23

Table S4. Devices parameters of SD all-PSCs based on PTzBI-oF and PS1 with different thicknesses at optimized DBE contents.

Thickness (nm)		V_{OC} (V)	J_{SC} (mA/cm^2)	FF (%)	PCE (%)
PTzBI-oF	PS1				
40	50	0.901	22.17	68.91	13.77
40	60	0.903	22.18	70.70	14.16
40	70	0.907	20.85	71.58	13.55
50	50	0.910	23.21	69.79	14.74
50	60	0.906	23.18	72.35	15.21
50	70	0.909	22.62	71.33	14.68
60	50	0.907	22.49	70.76	14.43
60	60	0.908	21.77	71.84	14.20
60	70	0.907	21.93	70.98	14.12

Table S5. The hole and electron mobilities measured by SCLC method for PTzBI-oF:PS1 blends constructed by BC and SD methods.

Devices	μ_h (cm^2 V^{-1} s^{-1})	μ_e (cm^2 V^{-1} s^{-1})
SD (as-cast)	3.22×10^{-4}	4.18×10^{-4}
SD (optimized)	1.36×10^{-3}	7.31×10^{-4}
BC (optimized)	9.13×10^{-4}	4.68×10^{-4}

Table S6. Relative parameters obtained from corresponding graphs.

Device	R_0 (Ω)	R_1 (kΩ)	τ_{TPC} (μs)	τ_{TPV} (μs)	$P(E,T)$ (%)	n (V_{OC}–P_{light})	α (J_{SC}–P_{light})
SD (as-cast)	94.15	77.95	0.43	1.51	73.10	1.60	0.86
SD (DBE)	22.15	106.04	0.15	6.37	94.18	1.21	0.96
BC (DBE)	28.56	71.39	0.31	3.42	93.72	1.29	0.89
SD (DBE), aged	20.93	96.30	0.15	6.27	92.30	1.28	0.95
BC (DBE), aged	30.52	55.11	0.53	1.99	85.45	1.37	0.85

Table S7. The curve fitting detail results of lamellar stacking and π-π stacking reflections

Detail	Type	Location	Area	FWHM	Sector
SD (as-cast)	Lorentzian	0.28	10.70	0.088	IP
	Gauss	1.50	4.31	0.528	OOP
	Lorentzian	1.69	15.76	0.307	
SD (DBE)	Lorentzian	0.28	11.68	0.087	IP
	Gauss	1.53	5.34	0.466	OOP
	Lorentzian	1.69	17.21	0.291	
BC (DBE)	Lorentzian	0.27	10.52	0.094	IP
	Gauss	1.50	4.77	0.567	OOP
	Lorentzian	1.70	13.49	0.287	

Table S8. Curves fitting results pole figures for the π-π stacking reflections.

Detail	Type	Location	Area	FWHM
SD (as-cast)	Gauss	90.55	38.41	52.81
SD (DBE)	Gauss	90.26	38.05	47.56
BC (DBE)	Gauss	90.32	33.82	47.85

References

[1] Peng F, An K, Zhong W, et al. A universal fluorinated polymer acceptor enables all-polymer solar cells with >15% efficiency. ACS Energy Lett, 2020, 5, 3702

[2] Zhu C, Li Z, Zhong W, et al. Constructing a new polymer acceptor enabled non-halogenated solvent-processed all-polymer solar cell with an efficiency of 13.8%. Chem Commun, 2021, 57, 935